

Title	Progress in airborne ultrasonic data communications for indoor applications
Authors	Jiang, Wentao;Wright, William M. D.
Publication date	2017-01-19
Original Citation	Jiang, W. and Wright, W. M. D. (2017) 'Progress in airborne ultrasonic data communications for indoor applications', IEEE 14th International Conference on Industrial Informatics (INDIN), Poitiers, France, 19-21 July. doi:10.1109/INDIN.2016.7819180
Type of publication	Conference item
Link to publisher's version	10.1109/INDIN.2016.7819180
Rights	© 2017, IEEE. Personal use of this material is permitted. Permission from IEEE must be obtained for all other uses, in any current or future media, including reprinting/republishing this material for advertising or promotional purposes, creating new collective works, for resale or redistribution to servers or lists, or reuse of any copyrighted component of this work in other works.
Download date	2024-03-03 15:52:31
Item downloaded from	https://hdl.handle.net/10468/5551



UCC

University College Cork, Ireland
Coláiste na hOllscoile Corcaigh

Progress in Airborne Ultrasonic Data Communications for Indoor Applications

Wentao Jiang and William M. D. Wright
School of Engineering - Electrical and Electronic Engineering
University College Cork, Cork, Ireland
Email: w.jiang@umail.ucc.ie, bill.wright@ucc.ie

Abstract—Capacitive ultrasonic transducers are efficient transmitters and receivers for ultrasonic waves in air, making them ideal devices for signal transmissions in air. Ultrasonic signals are unregulated, difficult to intercept from outside the room, and interference free to most electronic devices. These high security features make ultrasonic communication systems an alternative to radio frequency (RF) based systems for indoor applications. This paper investigated a prototype ultrasonic communication system using a pair of commercially available capacitive ultrasonic transducers in an indoor laboratory environment. Multichannel On-OFF keying (OOK) and binary phase-shift keying (BPSK) modulation schemes were implemented successfully in the system with wireless synchronization, achieving an overall data rate of 60 kb/s using ultrasonic bands from 50 to 110 kHz. The results show that a reliable line-of-sight (LOS) link can be established for communications over distances of 10 and 11 m using multichannel OOK and BPSK, respectively.

I. INTRODUCTION

Short range wireless communication technology has existed for years, and it has become an essential feature for most new electronic products due to its flexibility and remote control without expensive cabling. However, most emerging wireless devices are connected through radio frequency (RF) electromagnetic waves [1]. This leads to capacity issues in the RF spectrum and interference between different electronic equipment. In addition, RF signals can be intercepted remotely due to their penetrative nature [2]. Unlike the RF band, ultrasonic signal transmissions are regulation free and do not interfere with most electronic devices, thus eliminating any potential conflict with existing RF systems. Moreover, ultrasonic waves do not easily penetrate through solid barriers and do not travel great distances in air [3], [4]. Therefore, an indoor airborne ultrasonic system is inherently more secure with respect to malicious interventions from outside the room.

A variety of ultrasonic communication systems used for indoor positioning and localization have been reported in the literature [5], [6], [7], [8]. Compared with RF based systems, ultrasonic systems can provide more accurate measurement of time-of-flight (TOF) for location estimation at low cost, owing to the low propagation speed of ultrasonic waves in air. The first commercial use of airborne ultrasound was a wireless television remote control in 1950s [3]. By striking aluminium

rods, ultrasound waves with different frequencies can be produced to change the channel and the volume. Recently, another commercial ultrasonic system Shopkick [9] saw a huge success in the United States. Exclusive deals carried by ultrasonic signals generated by beacons installed in partner stores can be detected by customers' mobile phone microphones. Therefore, member users can only receive promotion codes by physically walking into the stores. Other airborne ultrasonic systems looked at implementing a computer input device containing a writing instrument coupled to ultrasonic transmitters which allow the system to continuously determine the position of the stylus [10]. In [11], a touchless human computer interface has been designed with a plurality of ultrasonic transducers as user input devices. Another recent work proposed a prototype networking framework for wearable medical devices based on ultrasonic communications [12]. To meet the privacy and security requirements, the health information of a patient can be collected and transmitted through an ultrasonic link. Other works have also investigated ultrasonic communication systems for digital data transmission. For instance, a wireless keyboard link using binary frequency-shift keying (BFSK) modulated ultrasonic signals has been proposed [13]. In this work, an error-free transmission range of 2.1 m was achieved with a system data rate of 83 kb/s using a pair of custom made broadband ultrasonic transducers. In [14], the authors studied the performance of single-channel quadrature phase shift keying (QPSK) modulated ultrasonic in-air transmission over a line-of-sight (LOS) link using the same air-coupled transducers as in [13]. The proposed solution achieved a higher data rate of 200 kb/s at 1.2 m with an effective bandwidth of 350 kHz. Later work developed a 2-carrier ultrasound transmission system on an embedded system using commercially available piezoelectric transducer pairs, achieving a data rate of 5.7 kb/s over distances up to 18 m, however, with a packet error rate of 13% [15].

This paper proposes a prototype airborne ultrasonic data communication system using multichannel modulation schemes with a pair of commercially available narrow bandwidth capacitive transducers to achieve a practical transmission range with a reasonable data transfer rate. In section II, how the system was implemented is described including signal design, transmission, synchronization and detection schemes. Section III introduced the apparatus and the experimental setup

of the work. This is followed by the experimental results and conclusions in Section IV and Section V, respectively.

II. SYSTEM DESCRIPTION

A. Signal design

In digital communications, a sequence of transmitted data symbols can be denoted as $\{d_k\}$, $k = -\infty, \dots, \infty$. The transmitted signal $s(t)$ with linear modulation is then given by

$$\begin{aligned} s(t) &= h_T(t) * \sum_{k=-\infty}^{\infty} d_k \delta(t - kT) \\ &= \sum_{k=-\infty}^{\infty} d_k h_T(t - kT) \end{aligned} \quad (1)$$

where T is the symbol interval, $h_T(t)$ is the impulse response of the transmit filter and $\delta(t)$ is the Dirac delta function. The modulator can be regarded as a pulse-shape filter and the impulse response of this filter is therefore rectangular of duration T . Baseband modulation methods chosen were on-off keying (OOK) and binary phase shift keying (BPSK). For OOK modulation, a positive pulse is obtained if the input data is “1” while a zero amplitude pulse is sent when a bit “0” occurs. For BPSK, positive pulses and negative pulses are used to convey information bits “1”s and “0”s. All the pulses are then summed at the output of the filter. As a result, the filter produces a baseband transmitted signal. However, sharp transitions occur when rectangular pulse filtering is applied. It leads to significant spectral leakage and thus produces severe interference to other sub-channel signals operating at neighbouring frequencies. Therefore, in pursuit of utilizing the limited bandwidth more efficiently and eliminating adjacent channel interference, introducing a proper pulse shaping technique is necessary to improve the signal transmission. In practise, the pulse shape filter with the following frequency response is often used [16]:

$$H_T(f) = \begin{cases} T, & |f| \leq \frac{1-\alpha}{2T} \\ \frac{T}{2} \{1 + \cos[\frac{\pi T}{\alpha} (|f| - \frac{1-\alpha}{2T})]\}, & \frac{1-\alpha}{2T} \leq |f| \leq \frac{1+\alpha}{2T} \\ 0, & \text{otherwise} \end{cases} \quad (2)$$

where α , ranging from 0 to 1, is a design parameter called the roll-off factor. This spectrum $H_T(f)$ is called the raised-cosine spectrum. The corresponding impulse response in the time domain is

$$h_T(t) = \text{sinc}\left(\frac{t}{T}\right) \frac{\cos\left(\frac{\alpha\pi t}{T}\right)}{1 - \left(\frac{2\alpha t}{T}\right)^2}. \quad (3)$$

The roll-off factor α defines the shape of the impulse response as well as the shape of the frequency response. A value of $\alpha = 0$ gives a rectangular-shaped spectrum with the narrowest bandwidth and $h_T(t)$ becomes a sinc. As the value of α increases from 0 to 1, the effective bandwidth also increases and the rate of decay becomes faster in the time

domain. Thus, by choosing a proper value of α , most of the channel power can be effectively limited to specific defined bandwidth. After the transmit filter, all the sub-channel signals at individual frequencies were linearly added together, giving a single waveform.

B. Signal transmission

When designing an airborne ultrasonic communication system, it is important to note that the propagation of ultrasound in air is intrinsically different from that of electromagnetic waves. One critical factor that limits the ultrasonic signal transmission range in air is the atmospheric absorption loss. The absorption coefficient α measured in dB/m can be calculated by [17]

$$\begin{aligned} \alpha &= f^2 \left[1.59 \times 10^{-10} \left(\frac{P_0}{P}\right) \left(\frac{T}{T_0}\right)^{\frac{1}{2}} \right. \\ &\quad \left. + 0.111 \left(\frac{T}{T_0}\right)^{-\frac{5}{2}} \frac{e^{-\frac{2239.1}{T}}}{f_{r,O} + \frac{f^2}{f_{r,O}}} + 0.929 \frac{e^{-\frac{3352}{T}}}{f_{r,N} + \frac{f^2}{f_{r,N}}} \right]. \end{aligned} \quad (4)$$

Here, f presents the sound frequency, P is the measured atmospheric pressure, P_0 is the standard pressure (101.325 kPa), T and T_0 are measured atmospheric temperature (in K) and standard temperature (293.15 K), respectively. The terms $f_{r,O}$ and $f_{r,N}$ are, respectively, the scaled relaxation frequencies for oxygen and nitrogen in Hertz. The values of the two frequencies depend on the measured temperature, relative humidity and atmospheric pressure [18]. Fig. 1 illustrates the absorption coefficient, α , as a function of relative humidity and temperature across the frequency ranges from 1 kHz to 1 MHz. As can be seen, at all different humidity and temperature conditions, low frequencies are relatively unaffected, while higher frequencies suffer significant attenuation which may cause severe distortion on received signals. This effect will become worse with an increase of the propagation distance. Therefore, for ultrasonic communications in air, the effective bandwidth is suppressed dramatically at high frequencies and may constrain the overall system data rate at long distances.

Another factor that contributes to ultrasonic attenuation is the beam spreading loss. Due to diffraction effects, the sound beam diverges when coming out of the transducer aperture. The angle of divergence, θ , can be expressed as [19]

$$\sin(\theta) = 1.22\lambda/D \quad (5)$$

where λ and D are the signal wavelength and the diameter of the transducer aperture, respectively. It is obvious from (5) that different amounts of the transmitted energy will be detected by the receiver depending on the transmission range. On the other hand, less energy will be intercepted by a receiver with the same diameter as the transmitter from a low-frequency signal than from a high-frequency signal at the same range before considering ultrasonic absorption in air.

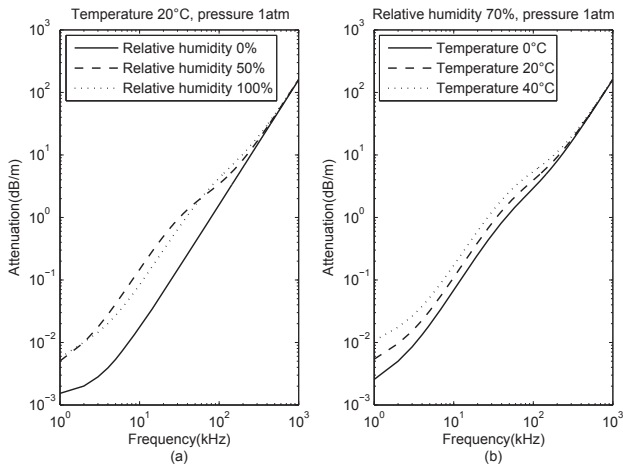


Fig. 1. Atmospheric absorption attenuation (a) as a function of frequency and relative humidity at 20°C and 1 atm pressure and (b) as a function of frequency and temperature at 70% relative humidity and 1 atm pressure.

C. Synchronization

Once an ultrasonic signal packet is detected, it is critically important for the receiver to identify the starting point of the arriving packet. A data-aided (DA) synchronization technique was used in the work. It is based on a known pilot signal being transmitted in front of the information data packets. As widely used in practical radar systems for range detection, a linear frequency modulation (LFM) signal whose frequency sweeps from low to high within a certain time is used as the pilot [20]. The DA technique is capable of providing the best estimation accuracy because it uses the maximum information about the transmitted signal. By performing the correlation of a known LFM pilot and the received signal using a matched filter at the receiver, the maximum energy of the matched filter output then indicates the start of the arriving data sequence.

D. Detection

The system detection and demodulation for both multichannel OOK and BPSK are depicted in Fig. 2. The received signal $R(t)$ was bandpass filtered by a Butterworth filter to extract the sub-channel signals at different frequencies. For OOK signals, the individual envelopes of the filtered sub-channel signals were detected using a Hilbert transform [21] before being decoded by bit comparators. For BPSK demodulation, the bandpass filtered signals were multiplied by their coherent reference carriers with the corresponding frequencies at each sub-channel. The resultant waveform was low-pass filtered and then decoded by a bit judger. All decoded bits were finally combined in a single sequence using a bit joiner.

III. APPARATUS AND EXPERIMENTAL SETUP

The experiment was conducted using a pair of commercially available SensComp series 600 capacitive ultrasonic transducers [22]. These transducers are constructed from a gold coated polymer membrane stretched across a round grooved aluminium back plate, and are designed for operating at an ultrasonic frequency of 50 kHz with a beam angle of 15°

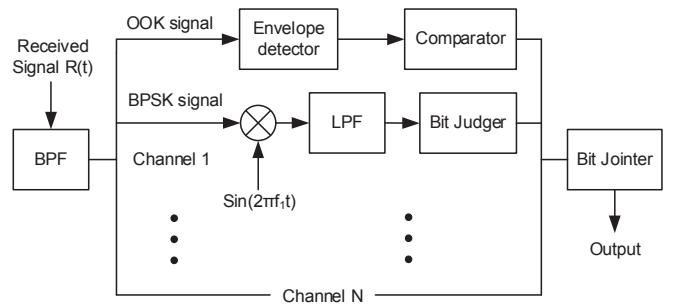


Fig. 2. Schematic diagram of the multi-channel on-off keying (OOK) and binary shift keying (BPSK) demodulator.

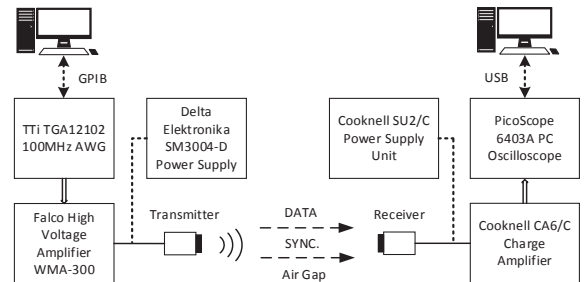


Fig. 3. Schematic diagram of the experimental set-up.

at -6 dB. The use of a flexible metallised membrane and a rigid back plate has allowed the frequency response of these transducers to be increased well into the ultrasonic region [23]. The trapped air between the membrane and the back plate acts as a natural spring and thus improves the sensitivity and produces a wider bandwidth, making the device highly suitable for air-coupled applications.

Fig. 3 illustrates the experimental setup of the ultrasonic communication system. The data to be transmitted were encoded and modulated using MATLAB (The Math Works, Inc.) before sending to a TTI TGA 12102 arbitrary waveform generator (Thurlby Thandar Instruments Ltd.) via a GPIB interface. The voltage signal was then amplified by a Falco WMA-300 amplifier (Falco Systems B.V.) and superimposed by +200 V dc bias generated by a Delta Elektronika SM3004-D power supply (Delta Elektronika B.V.). The receiver was connected to a Cooknell CA6/C charge amplifier (Cooknell Electronics Ltd.) powered by its SU2/C power supply unit and followed by a PicoScope 6403A PC oscilloscope (Pico Technology). The signal waveforms were finally saved to another PC through a USB interface for off-line signal processing.

By sending a pulse signal generated by a Panametrics 500PR pulser (Panametrics, Inc.) from the transmitter to the receiver through an air gap of 1 m, the measured system frequency and phase response are shown in Fig. 4(a) and Fig. 4(b), respectively. As can be seen from Fig. 4(a), the spectrum stands out and spreads across the ultrasonic bands from 48 to 112 kHz in terms of a 6-dB bandwidth as the dashed line indicates. The phase response of the channel is nearly linear across the 6-dB bandwidth as shown in

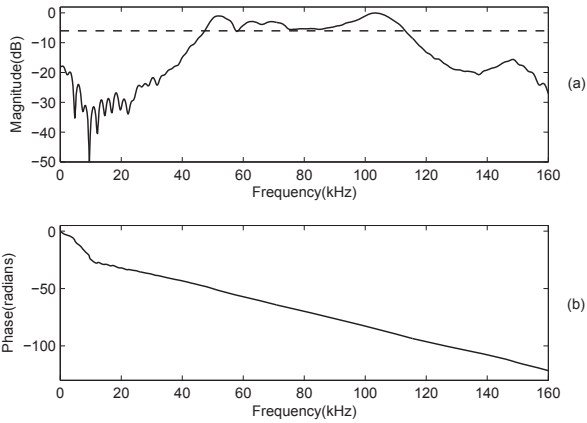


Fig. 4. System characteristics: (a) system response and (b) phase response.

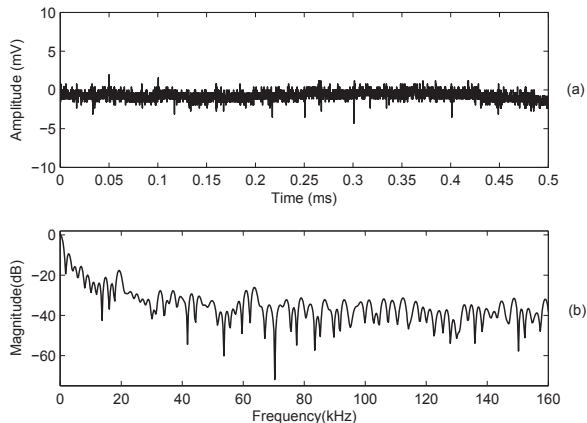


Fig. 5. Background noise in: (a) time domain and (b) frequency domain.

Fig. 4(b). In addition, to analyse the background noise, a signal was captured by sending no data from the transmitter transducer as Fig. 5(a) shows. Accordingly, its frequency spectra is illustrated in Fig. 5(b). As can be seen, within the audio frequency range, the magnitude response is relatively higher. But it stays relatively constant afterwards, extending to ultrasonic frequencies. Therefore, most ambient noise is audio noise which can be easily filtered out. Note that the recorded impulse signal amplitude was about 7.77 mV rms and the background noise level stayed approximately at 0.92 mV rms, giving a signal-to-noise ratio (SNR) of 18.52 dB at this range.

IV. RESULTS

The experiments were carried out in an indoor laboratory environment with measured room temperature at 20°C and relatively humidity of around 72%. The basic signal parameter settings were listed in Table I. According to the system frequency response illustrated in Fig. 4(a), six channels from 50 to 110 kHz with a channel spacing of 12 kHz were used. The bit duration was set at 0.1 ms, thus the sub-channel bit rate was 10 kb/s. Since there are six channels transmitted in parallel, the overall data rate achieved was at 60 kb/s.

TABLE I
PARAMETERS OF THE SIGNALS USED IN THE EXPERIMENT

Parameters	Settings
Sampling rate	$f_s = 10$ MHz
Signal bandwidth	$BW = 60$ kHz
Bit duration	$T = 0.1$ ms
Sub-channel spacing	$f_d = 12$ kHz
Number of sub-channels	$N = 6$

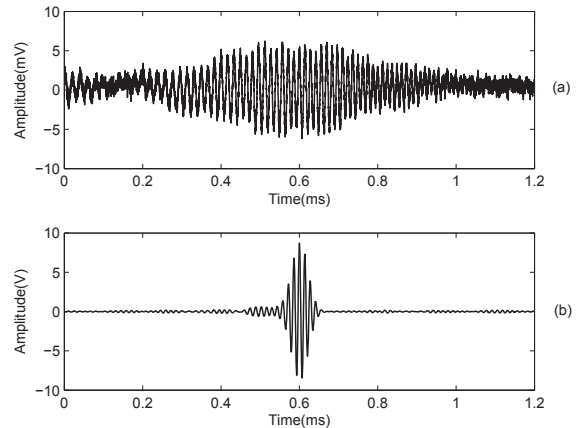


Fig. 6. Wireless synchronization: (a) received LFM signal at 10 m and (b) its matched filter output.

Fig. 6(a) shows a received Hamming-windowed LFM synchronization signal at 10 m with very low SNR. The signal had a duration of 1 ms with its frequency swept from 50 to 100 kHz. By performing cross-correlation of a known signal and the received signal in noise using a matched filter, the resulting waveform in Fig. 6(b) shows a large enhancement of SNR which enables a precise and robust detection of the starting point of the incoming signal packets.

To analyse the effects of pulse shaping technique on airborne ultrasonic signal transmission, the received 6-channel OOK and BPSK signals at 5 m with and without pulse shaping and their frequency spectra are illustrated in Fig. 7. In the time domain, there is visually little difference between the unshaped and pulse shaped signals as shown in Fig. 7(a) and (b). However, compared with the unshaped signal spectrum in Fig. 7(c), the sidelobes of the pulse-shaped signal spectrum in Fig. 7(d) have been reduced by about 10 dB, thus reducing both inter-symbol interference (ISI) and inter-channel interference (ICI). The received unshaped and pulse-shaped 6-channel BPSK signals in Fig. 7(e) and (f) present more constant envelopes, as expected. Again, the pulse-shaped signal shows a more concentrated spectrum in Fig. 7(h), with reduced and smoothed sidelobes. It is noted that negative slopes along the frequency axis can be observed for both OOK and BPSK spectra, this is because high frequency channel signals suffer more ultrasonic attenuation at the 5-m transmission range.

The demodulation and decoding process of both multichannel OOK and BPSK at 5 m are presented in Fig. 8 and

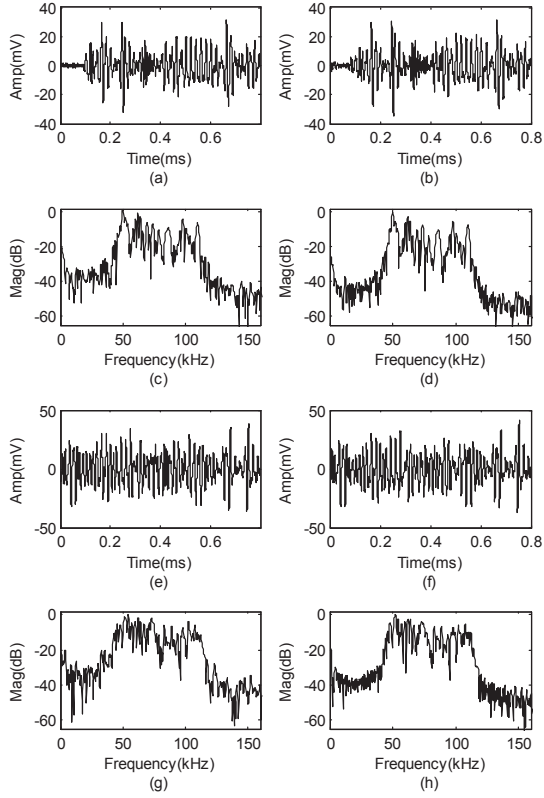


Fig. 7. Received time domain 6-channel OOK signals at a transmission distance of 5 m: (a) unshaped ($\alpha = 1$) and (b) $\alpha = 0$ and their spectra (c) and (d), and received time domain 6-channel BPSK signals at a transmission distance of 5 m: channels at 5 m (e) unshaped ($\alpha = 1$) and (f) $\alpha = 0$ and their spectra (g) and (h).

Fig. 9, respectively. As can be seen from Fig. 8(a), the logic “1”s and “0”s of the bandpass filtered OOK signal can be visually identified. Afterwards, the absolute value of the signal envelope was obtained and plotted in Fig. 8(b). Fig. 8(c) presents the bar plot of the normalised energy under the curve of each bit duration. In order to minimise the effects of energy leakage, only the central 20% of the energy was calculated. It was then compared with a threshold value of 0.28 derived by trial and error. For multichannel BPSK demodulation, the opposite phases for “1”s and “0”s are clearly displayed after coherent multiplication as shown in Fig. 9(b). By applying a lowpass filter, it is then straightforward to decode the received bits based on the resulting curve as illustrated in Fig. 9(c).

System reliability was evaluated based on the bit error rate (BER) tests at different ranges up to 11 m with different roll-off factors from 0 to 1 with an increment of 0.2. Thus, 57600 randomly generated binary bits were OOK and BPSK modulated and transmitted through the air channel. It was found that with roll-off factors of 0 and 0.2 for OOK and BPSK respectively, the lowest bit errors were detected at all ranges. The transmission ranges with no measurable errors for multichannel OOK and BPSK were up to 10 m and 11 m, respectively. To better visualise the signal conditions, eye diagrams of the received OOK signals over the lowest and

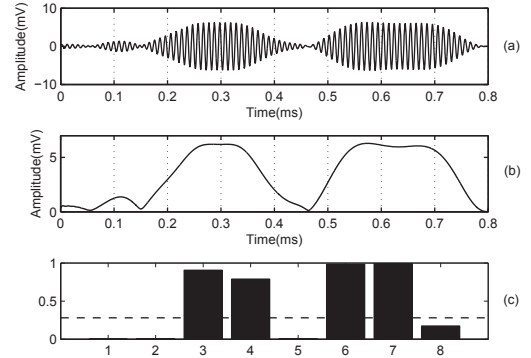


Fig. 8. Demodulation and decoding of multichannel OOK signals at 5 m: (a) bandpass filtered 98 kHz channel signal, (b) envelope of the signal in (a) and (c) normalised energy bar plot under the curve of each bit duration.

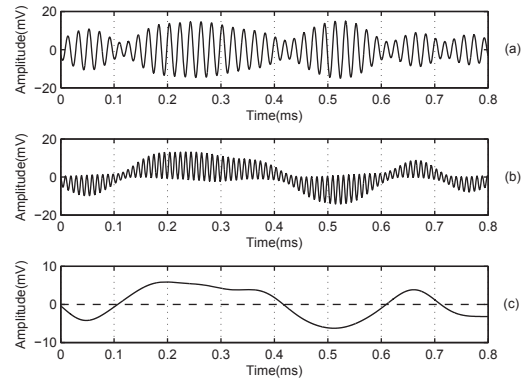


Fig. 9. Demodulation and decoding of multichannel BPSK signals at 5 m: (a) bandpass filtered 50 kHz channel signal, (b) waveform after coherent multiplication and (c) lowpass filtered signal of the waveform in (b).

the highest channels at ranges of 5 and 10 m are illustrated in Fig. 10. As can be seen, over 5 m, both the 50 and 110 kHz OOK signals have larger amplitudes and more open eyes in Fig. 10(a) and (b) than those of the signals received at a longer range (10 m) in Fig. 10(c) and (d). The bit errors started to occur on the 110 kHz channel signal at 10 m as its eye is about to close due to ultrasonic attenuation in air as shown in Fig. 10(d). Accordingly, the eye diagrams of the BPSK signals over 50 and 110 kHz channels at 5 and 11 m are presented in Fig. 11. As can be seen, short range (5 m) BPSK signals at both 50 and 110 kHz channels in Fig. 11(a) and (b) have better eye shapes with less jitter and amplitude variations compared to long range (11 m) 50 and 110 kHz channel signals in Fig. 11(c) and (d). The eye of the 110 kHz signal at 11 m in Fig. 11(d) is completely closed, therefore introducing most of the bit errors at this range.

V. CONCLUSIONS

This work investigated airborne ultrasonic data communications using 6-channel OOK and BPSK modulation schemes in an indoor environment. A pair of commercially available SensComp capacitive ultrasonic transducers at 50 kHz were used for the in-air transmission, achieving an overall sys-

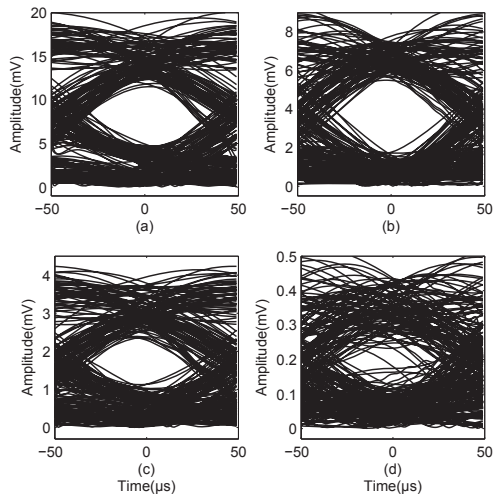


Fig. 10. Eye diagrams for OOK signals in 50 kHz (a) and 110 kHz (b) channels at 5 m and signals in 50 kHz (c) and 110 kHz (d) channels at 10 m.

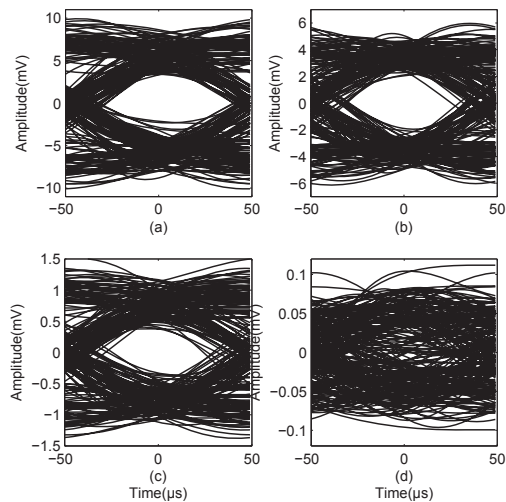


Fig. 11. Eye diagrams for BPSK signals in 50 kHz (a) and 110 kHz (b) channels at 5 m and signals in 50 kHz (c) and 110 kHz (d) channels at 11 m.

tem data rate of 60 kb/s with a bandwidth efficiency of 1 b/s/Hz. Wireless synchronization was performed by sending a LFM signal before the data packets. The experimental results demonstrated the robustness of the proposed communication system with error-free decoding transmission distances up to 10 m and 11 m by using multichannel OOK and BPSK modulations, respectively. However, diffractions and reflections may occur in a non-LOS setup, which will degrade the system transmission range and achieved data rate. These effects will be investigated in future work.

ACKNOWLEDGMENT

This work was supported by Science Foundation Ireland (SFI) Research Frontiers Programme grant number 11/RFP.1/ECE3119.

REFERENCES

- [1] R. Kraemer and M. Katz, *Short-Range Wireless Communications: Emerging Technologies and Applications*, ser. WILEY-WWRF SERIES. Wiley, 2009.
- [2] N. Borisov, I. Goldberg, and D. Wagner, "Intercepting mobile communications: the insecurity of 802.11," in *Proceedings of the 7th annual international conference on Mobile computing and networking*, ser. MobiCom '01. New York, NY, USA: ACM, 2001, pp. 180–189.
- [3] R. Adler, P. Desmares, and J. Spracklen, "An ultrasonic remote control for home receivers," *Consumer Electronics, IEEE Transactions on*, vol. CE-28, no. 1, pp. 123–128, Feb 1982.
- [4] D. Schindel and D. Hutchins, "Applications of micromachined capacitance transducers in air-coupled ultrasonics and nondestructive evaluation," *Ultrasonics, Ferroelectrics, and Frequency Control, IEEE Transactions on*, vol. 42, no. 1, pp. 51–58, Jan 1995.
- [5] S. Holm, "Airborne ultrasound data communications: the core of an indoor positioning system," in *Ultrasonics Symposium, 2005 IEEE*, vol. 3, Sept 2005, pp. 1801–1804.
- [6] M. Hazas and A. Hopper, "Broadband ultrasonic location systems for improved indoor positioning," *Mobile Computing, IEEE Transactions on*, vol. 5, no. 5, pp. 536–547, May 2006.
- [7] M. Saad, C. J. Bleakley, T. Ballal, and S. Dobson, "High-accuracy reference-free ultrasonic location estimation," *Instrumentation and Measurement, IEEE Transactions on*, vol. 61, no. 6, pp. 1561–1570, June 2012.
- [8] S. Lopes, J. Vieira, and D. Albuquerque, "High accuracy 3d indoor positioning using broadband ultrasonic signals," in *Trust, Security and Privacy in Communications (TrustCom), 2012 IEEE 11th International Conference on*, June 2012, pp. 2008–2014.
- [9] (2016, May.) The Shopkick website. [Online]. Available: <http://www.shopkick.com/>
- [10] M. Stefik and J. Heater, "Ultrasound position input device," U.S. Patent 4,814,552, Mar. 21, 1989.
- [11] Z. Radivojevic, Y. Zou, K. Wang, R. Takala, V. Lantz, R. Lehtiniemi, J. Rantala, and R. Vatanparast, "Apparatus, methods and computer program products providing finger-based and hand-based gesture commands for portable electronic device applications," U.S. Patent 8,086,971, Dec. 27, 2011.
- [12] G. E. Santagati and T. Melodia, "U-wear: Software-defined ultrasonic networking for wearable devices," in *Proceedings of the 13th Annual International Conference on Mobile Systems, Applications, and Services*, ser. MobiSys '15. New York, NY, USA: ACM, 2015, pp. 241–256.
- [13] C. Li, D. Hutchins, and R. Green, "Short-range ultrasonic digital communications in air," *Ultrasonics, Ferroelectrics and Frequency Control, IEEE Transactions on*, vol. 55, no. 4, pp. 908–918, 2008.
- [14] —, "Short-range ultrasonic communications in air using quadrature modulation," *Ultrasonics, Ferroelectrics and Frequency Control, IEEE Transactions on*, vol. 56, no. 10, pp. 2060–2072, 2009.
- [15] A. Ens and L. Reindl, "Multicarrier airborne ultrasound transmission with piezoelectric transducers," *Ultrasonics, Ferroelectrics, and Frequency Control, IEEE Transactions on*, vol. 62, no. 5, pp. 905–914, May 2015.
- [16] J. Proakis and M. Salehi, *Digital Communications*. McGraw-Hill Higher Education, 2008.
- [17] W. Mason and R. Thurston, Eds., *Physical acoustics: principles and methods*, ser. Physical Acoustics. Academic Press, 1984.
- [18] H. E. Bass, L. C. Sutherland, A. J. Zuckerwar, D. T. Blackstock, and D. M. Hester, "Atmospheric absorption of sound: Further developments," *The Journal of the Acoustical Society of America*, vol. 97, no. 1, pp. 680–683, 1995.
- [19] J. Krautkrämer and H. Krautkrämer, *Ultrasonic testing of materials*. Springer-Verlag, 1990.
- [20] M. Skolnik, *Introduction to Radar Systems*, ser. Electrical engineering series. McGraw Hill, 2001.
- [21] Y. Shmaliy, *Continuous-time signals*. Springer, 2006.
- [22] (2016, Jan.) The SensComp Website. SensComp, Inc. [Online]. Available: <http://www.senscomp.com/pdfs/series-600-environmental-grade-sensor.pdf>
- [23] K. Nakamura, Ed., *Ultrasonic Transducers: Materials and Design for Sensors, Actuators and Medical Applications*. Woodhead Publishing Limited, 2012.